14th Australasian Fluid Mechanics Conference
Adelaide University, Adelaide, Australia
10-14 December 2001

# Two- and Three-Dimensional Temperature Structures in a Shallow Wedge Subject to Solar Radiation

Chengwang Lei and John C. Patterson

School of Engineering, James Cook University, Townsville, QLD 4811, Australia

**Abstract**

The temperature structures in a water-filled shallow wedge subject to solar radiation obtained from two-dimensional (2-D) and three-dimensional (3-D) simulations are presented in this paper. The 3-D results show that the flow experiences a transition from 2-D to 3-D as it passes through three stages of the flow development. A comparison between the 2-D and 3-D results indicates that the 2-D simulation reproduces major flow features at all stages irrespective of the three-dimensionality.

## Introduction

This study considers the natural convection in a water-filled shallow wedge subject to solar radiation. It is motivated by increasing interests in understanding the diurnal circulations in the littoral regions of lakes which play an important role in promoting exchange of water properties in these regions [1,3,7]. However, the present study focuses on very shallow waters instead of large-scale lakes, and thus one may also find it relevant to solar collectors, solar ponds or other facilities utilising solar energy.

The authors have previously reported results for this problem obtained from a two-dimensional (2-D) numerical simulation [5]. In that study, the transient flow development starting from an isothermal and stationary state is investigated. The 2-D simulation has revealed three distinct stages of the flow development, namely an initial stage, a transitional stage and a quasi-steady stage. The initial stage is characterised by rapid growth of a thermal boundary layer along the sloping bottom due to heat conduction from the bottom, which absorbs penetrative radiation reaching that depth. The transitional stage is characterised by the presence of instabilities emanating from the bottom boundary which are manifested as rising plumes translating up the slope. The quasi-steady state is characterised by a steady rise in average temperature and intermittent presence of instabilities with reduced intensities. The 2-D simulation has also confirmed earlier experimental observations using a shadowgraph technique [6]. However, the application of a 2-D model for an essentially three-dimensional (3-D) experiment has limited the accountability of the numerical simulation.

In this study, the transient flow development in a shallow wedge subject to solar radiation is reinvestigated numerically by solving the full 3-D governing equations. The temperature structures in the wedge are discussed, and the results of 2-D and 3-D calculations are compared.

## Formulation and Numerical Procedures

For the 3-D simulation, a wedge of length $L$, width $W$ and maximum depth $h$ (the bottom slope is $A = h/L$) with rigid non-slip boundaries at the bottom and end and an open boundary at the top is considered. The wedge is filled with water initially at rest and at temperature $T_0$. At time $t = 0$, a surface radiation of intensity $I_0$ is initiated and thereafter maintained. When the radiation travels through a water column, the radiation intensity at a particular wavelength decreases with depth according to Beer's law [1,8]:

$$I = I_0 e^{\eta y} \quad for \quad y \le 0 \tag{1}$$

where $I$, is the radiation intensity at a given depth, $y$ the negative water depth and $\eta$, the bulk attenuation coefficient of water. The shallow wedge assumption implies that the water depth is less than the attenuation length of radiation, ie. $h < \eta^{-1}$. In this case, a significant amount of radiation reaches the sloping bottom. It is assumed that any residual radiation reaching the bottom is fully absorbed by the bottom, and the energy is then released back to the water in the form of boundary heat flux [1]. Accordingly, the temperature boundary condition at the bottom is given by

$$\partial T/\partial n = -(H_0/k)e^{-A\eta x} \quad for \quad y = -Ax \tag{2}$$

where $T$, is temperature, $n$ the direction normal to the slope, $H_0$ the volumetric surface heating given by $H_0 = I_0/(\rho_0 C_p)$, $\rho_0$, $C_p$ and $k$ are respectively the density, specific heat and thermal diffusivity for water at $T_0$, $x$ the distance from the tip.

The flow and temperature changes within the wedge are then governed by the 3-D Navier-Stokes equations and energy equation with Boussinesq assumptions:

$$u_t + uu_x + vu_y + wu_z = -\rho_0^{-1} p_x + \nu\nabla^2 u \tag{3}$$

$$v_t + uv_x + vv_y + wv_z = -\rho_0^{-1} p_y + \nu\nabla^2 v + g\beta(T - T_0) \tag{4}$$

$$w_t + uw_x + vw_y + ww_z = -\rho_0^{-1} p_z + \nu\nabla^2 w \tag{5}$$

$$T_t + uT_x + vT_y + wT_z = k\nabla^2 T + H_0\eta e^{\eta y} \tag{6}$$

$$u_x + v_y + w_z = 0 \tag{7}$$

where $u$, $v$ and $w$ are the velocity components in the horizontal, vertical and transverse directions, $x$, $y$ and $z$ are the corresponding coordinates, $p$ pressure, $g$ acceleration due to gravity, $\beta$ and $\nu$ are respectively the coefficient of thermal expansion and kinematic viscosity for water at $T_0$. The second term on the right hand side of the energy equation (6) quantifies the absorption of radiation by the water (see also [1]).

The temperature and velocity boundary conditions for the 3-D simulation are the same as those for the 2-D simulation (refer to [5] for details) except that additional periodic conditions are prescribed in the transverse direction in the 3-D case.

Since the water body in the wedge is heated continuously by radiation, and there is no heat loss through the boundaries, the water temperature will keep increasing without a limit, and there will be no steady state in terms of temperature. However, with a constant surface radiation being applied, a quasi-steady state may be reached in which the temperature gradients and flow velocities become steady. In the quasi-steady state, the temperature increases at the same rate everywhere in the tank, and the net increase of the temperature is a function of time. Therefore, the temperature can be split into two components, a spatially averaged temperature which increases in time and a spatially variable temperature which has a steady state spatial distribution after a transition. In this study, a quasi-steady temperature equation with respect to the spatially variable temperature (the non-dimensional form is given by Equation (11)) is solved. A comparison between Equations (6) and (11) shows that an additional heat sink ($2H_0/h$) is introduced in the temperature equation. This is to balance the linear growth of the

spatially averaged temperature. Details regarding the quasi-steady state simplification can be found in [5].

The quantities in the system equations comprising the Navier-Stokes equations and the quasi-steady temperature equation are normalised by the following scales: length scale: $x, y, z \sim h$; time scale: $t \sim h^2/k$; temperature scale: $(T - T_0) \sim H_0 h/k$; velocity scale: $u, v, w \sim k/h$; pressure gradient scale: $p_x, p_y, p_z \sim \rho_0 g\beta H_0 h/k$; attenuation coefficient scale: $\eta \sim h^{-1}$. The system equations are then rewritten in dimensionless forms as follows:

$$u_t + uu_x + vu_y + wu_z = -Pr^2 Grp_x + Pr\nabla^2 u \quad (8)$$

$$v_t + uv_x + vv_y + wv_z = -Pr^2 Grp_y + Pr\nabla^2 v + Pr^2 GrT \quad (9)$$

$$w_t + uw_x + vw_y + ww_z = -Pr^2 Grp_z + Pr\nabla^2 w \quad (10)$$

$$T_t + uT_x + vT_y + wT_z = \nabla^2 T + (\eta e^{\eta y} - 2) \quad (11)$$

$$u_x + v_y + w_z = 0 \quad (12)$$

where $Pr$ and $Gr$ are Prandtl and Grashof numbers defined as:

$$Pr = \nu/k \quad (13)$$

$$Gr = g\beta H_0 h^4 / \nu^2 k\,, \quad (14)$$

All quantities in Equations (8) ~ (12) are dimensionless. The corresponding 2-D model can be found in [5]. The 2-D and 3-D models are then solved using a finite difference method. Detail of the numerical procedures can be found in [4].

**Numerical Results**

2-D and 3-D calculations are now carried out in a triangular domain of dimensionless length of 10, width of 5 and depth of 1. The bottom slope is 0.1, and the dimensionless bulk attenuation coefficient is set to 0.37. The convective flow is calculated at a Grashof number $Gr = 2.51\times10^6$ and a Prandtl number $Pr = 6.83$. All these parameters are chosen from the experiment [6]. To avoid singularity at the tip in numerical calculations, the tip is cut off at $x = 1$, and an additional rigid non-slip and adiabatic wall boundary is assumed here. It is anticipated that the cut-off of the tip will not modify the flow significantly.

In the 2-D case, an 81×61 non-uniform structured mesh is constructed in the $(x, y)$ plane so that nodes are effectively clustered to the vicinities of all boundaries. A test of mesh and time-step dependence is conducted prior to the calculation by halving the grid spacing and time step simultaneously so that the CFL (Courant-Freidrich-Lewy) number remains the same. No significant difference in the numerical solutions has been noticed from the refinement of the mesh (refer to [5]). Therefore, the 81×61 mesh is used for the present calculation. In the 3-D case, the 3-D mesh is simply an extension of the 2-D mesh along the $z$ direction, in which nodes are equally spaced (recall that periodic boundary conditions apply in the transverse direction). The final mesh for the 3-D calculation is 81×61×41. A fixed time step of $10^{-6}$ is used throughout this study.

As reported in [5], three stages of the flow development can be identified from the numerical simulation. The present study is concerned with the temperature structures only, and the 2-D and 3-D temperature structures are compared here.

**Temperature Structure at the Early Stage**

The temperature structures within the wedge at the early stage after the initiation of the surface radiation are presented in Figure 1 with Figure 1a giving the iso-surfaces of temperatures obtained from the 3-D calculation and Figure 1b giving the temperature contours obtained from the 2-D calculation. Note that the temperature data presented here is obtained by solving the quasi-steady state temperature equations, in which a heat sink is introduced to balance the linear growth of the spatially averaged temperature with time. A negative value of temperature in the enclosure indicates a lower growth rate of the temperature relative to the mean growth across the tank, and a positive value indicates a higher growth rate relative to the mean growth. Therefore, it is the relative value rather than the absolute value of the temperature that is meaningful to subsequent discussions.

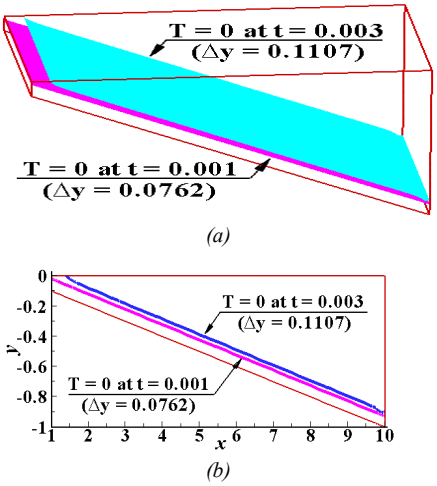


*Figure 1 Temperature structure at the early stage. (a) 3-D simulation. (b) 2-D simulation.*

The growth of a thermal boundary layer along the sloping bottom is clearly demonstrated by the temperature structures in Figure 1. It is observed from both 2-D and 3-D calculations that the temperature in a region close to the sloping bottom increases sharply at the early stage. This is due to the diffusion of heat flux from the sloping boundary, and thus indicates the growth of a thermal boundary layer. Apart from this boundary region which has positive temperatures, the temperatures in the rest of the enclosure are negative. Therefore, the location of the $T = 0$ iso-surface, which is indicated in Figure 1 (Δy is the distance above the bottom), approximately represents the boundary of the thermal layer. It is seen in Figure 1a that the iso-surface of $T = 0$ moves quickly away from the sloping bottom, indicating a rapid expansion of the thermal boundary layer. It is also found that the temperature variation in the negative region is negligible compared with that of the boundary region, suggesting that the bottom heating is dominating the radiation absorption by the water column at the early stage.

Figure 1a shows that the iso-surfaces of $T = 0$ are approximately parallel to the sloping bottom. This is also the case for all positive temperatures within the thermal boundary layer at this stage. Outside the thermal boundary layer, the iso-surfaces of temperatures are horizontal. Figure 1a also shows that the temperature structure is purely 2-D at the early stage, and thus is accurately captured by the 2-D simulation (Figure 1b). A quantitative examination of the positions of the $T = 0$ iso-surfaces and contours indicates that the 2-D and 3-D simulations follow closely until the early transitional stage (see the section below).

The growth of the thermal boundary layer generates a horizontal temperature gradient as well as an adverse vertical temperature gradient. The former is the initial driving force of a large-scale circulation in the enclosure, while the latter is the direct cause of the convective instability to be discussed below.

**Temperature Structure at the Transitional Stage**

While the surface radiation is maintained, the residual radiation continues to be absorbed by the bottom, and the energy continues to be released from the sloping bottom to the lower layer of the

water body. As a consequence, the thermal boundary layer continues to grow. Since this process generates an adverse temperature gradient in the thermal boundary layer, a Rayleigh-Bénard instability also develops while the thermal layer is growing. When the adverse temperature gradient is great enough, an instability will manifest itself as vertical convection. The convective instability is observed in the numerical simulations.

Figure 2 presents both 2-D and 3-D results showing the occurrence of rising thermals at the transitional stage. It is seen from the temperature iso-surface at $t$ = 0.01 (Figure 2a) that crests containing warm water are forming from the thermal boundary layer at different locations along the streamwise direction. These structures originate from the bottom thermal layer and are quickly amplified. They are eventually released from the thermal layer into the core flow and rapidly disperse into the upper cold layer. It is interesting to see in Figure 2a that the overall flow remains 2-D at this time despite of the onset of convective instability, and thus it is again accurately reproduced in the 2-D simulation (Figure 2b). The crest-like structures are different from the so-called plumes, which are typically 3-D. This is the early stage of the secondary convection, and it lasts only for a short time.

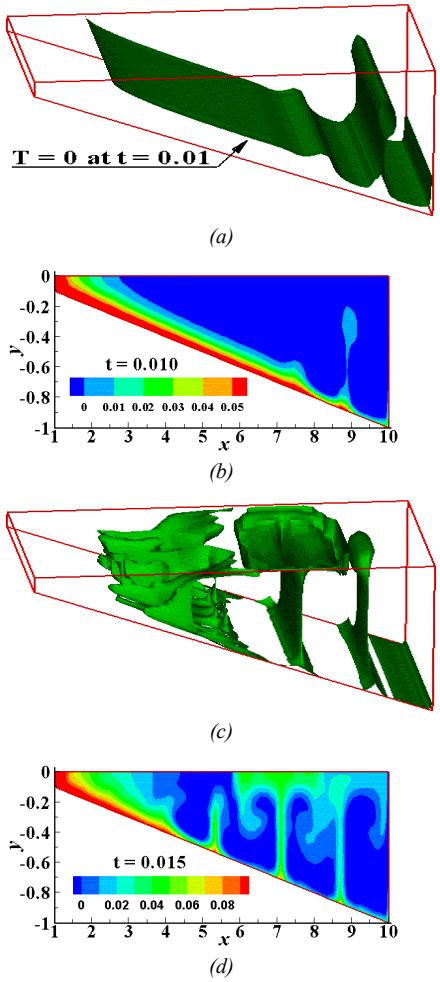


*Figure 2 Temperature structures after the onset of convective instability. (a) 3-D simulation, t = 0.010. (b) 2-D simulation, t = 0.010. (c) 3-D simulation, t = 0.015. (d) 2-D simulation, t = 0.015.*

At $t$ = 0.015 (Figure 2c), the 2-D secondary convection has now become 3-D, and it is very likely to form 3-D rising plumes, which are indeed observed at later times. Since the upper fluid layer is cold at this stage, the plumes are seen to penetrate through the entire local water depth. It is noteworthy that the burst of rising plumes is not regular; there are no fixed locations and frequencies in this process. In addition, it is observed that the rising plumes are carried by the primary circulation up the slope. Therefore, no stable configuration of the temperature structure will be reached. However, a quasi-steady state pattern will be reached at a certain stage (see Figure 3). Despite the three-dimensionality of the flow at this stage, the major features of the temperature structure are still closely reproduced in the 2-D simulation (Figure 2d), and the 2-D results have demonstrated qualitatively similar properties of the flow as the 3-D results.

**Temperature Structure at the Quasi-Steady State**

In the present case, the heat conducted into the thermal boundary layer is convected away from this layer by both the primary circulation and the secondary flow due to the convective instability. At a certain stage, the heat conduction and convection reach a balance, and the growth of the thermal boundary layer ceases. The horizontal temperature gradient in the thermal boundary layer will maintain a steady upwelling flow along the sloping bottom, while the vertical adverse temperature gradient will maintain a secondary motion. Therefore, a quasi-steady state is reached.

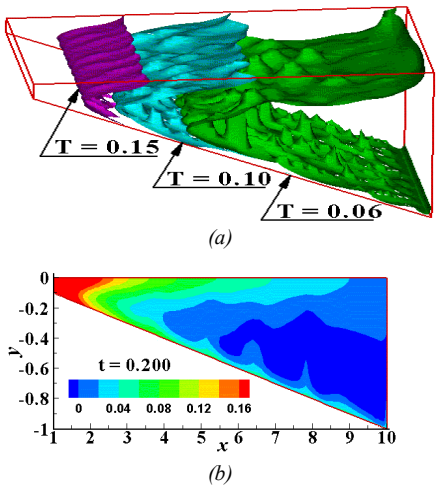


*Figure 3 Typical temperature structures at the quasi-steady state. (a) 3-D simulation, t = 0.2. (b) 2-D simulation, t = 0.2.*

The typical temperature structures at the quasi-steady state are shown in Figure 3, which presents the results obtained from both 2-D and 3-D calculations. At this stage, distinct horizontal temperature gradients are established in both the upper water layer and the thermal boundary layer. The overall flow structure does not change significantly. However, the detail of the flow structure is modified by the intermittent burst of rising thermals along the thermal boundary layer. The intermittent convection is governed by a cyclic process as described by [2]: the formation of a thermal boundary layer by diffusion, the destruction of the layer by convection and the reformation of the thermal boundary layer by diffusion. A comparison between Figures 2 and 3 shows that the intensity of the secondary convection is reduced at the quasi-steady stage. This is due to the development of a stabilising upper layer underneath the water surface, which tends to suppress the secondary convection. At this stage, the rising thermals disperse completely before reaching the water surface, in contrast to a penetration of the entire depth in the transient state.

With the existence of the secondary convection, the flow remains fully 3-D throughout the quasi-steady state (Figure 3a). It is interesting to see that the 2-D simulation still qualitatively captures the major features of the flow (Figure 3b). This is due to the isotropic features of the plumes in the $x$-$z$ plane. The 2-D

temperature structure plotted in Figure 3b can be interpreted as a slice within the ($x$, $y$) plane extracted from the 3-D structure (Figure 3a). Nevertheless, certain features such as the wavelength of the secondary motion in the transverse direction cannot be observed from the 2-D simulation.

A comparison between the 3-D results given in Figures 2 and 3 indicates that the secondary convection, comprising of more or less regularly spanned convection cells, is also well established at the quasi-steady stage. Clearly, the secondary convection in the upper water layer has a dominant wavelength along the transverse direction near both the shallow and deep ends (Figure 3a). In fact, there is also a dominant transverse wavelength for the entire thermal boundary layer. It is also seen in Figure 3a that the transverse wavelength for the upper layer increases along the streamwise direction. These 3-D features can be observed only from the 3-D simulation.

## Horizontal Heat Transfer

The horizontal heat transfer rate is a quantity of practical interests. It is defined in 2-D and 3-D domains respectively as (refer to [3])

$$H(x) = \int_{-Ax}^{0} \left( uT - \frac{\partial T}{\partial x} \right) dy \qquad (15)$$

$$H(x) = \frac{1}{W} \int_{0}^{W} \int_{-Ax}^{0} \left( uT - \frac{\partial T}{\partial x} \right) dydz \qquad (16)$$

where $H(x)$ is the horizontal heat transfer rate across a vertical sectional plane at a given $x$ location. Here, the dimensional quantity has been normalised by $I_0h$. It is then integrated along the horizontal direction as follows

$$H = \frac{1}{L} \int_{0}^{L} H(x)\, dx \qquad (17)$$

where $H$ is the average horizontal heat transfer rate.

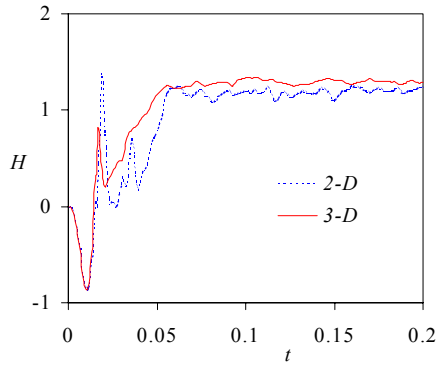


*Figure 4 Time series of horizontal heat transfer rate obtained from 2-D and 3-D simulations.*

The time histories of the averaged heat transfer rates obtained from both 2-D and 3-D simulations are plotted in Figure 4. Both plots indicate three stages of the flow development. Note that the two curves overlap at early times, supporting the premise that the early flow development is truly 2-D. It is seen in Figure 4 that there is a distinct dip in the time series of the horizontal heat transfer at early times. This is due to a strong up slope flow of warmer water and a weak return flow of cooler water at this stage. The horizontal heat transfer fluctuates after the dip, indicating the onset of the convective instability and the start of the transitional stage. Both 2-D and 3-D calculations predict that the switch from the initial stage to the transitional stage occurs at about $t$ = 0.011. In the transitional stage, the fluctuation of the heat transfer rate is strong and irregular. After a quasi-steady state is reached, the horizontal heat transfer oscillates about a stable mean value with reduced amplitude.

Figure 4 indicates that the quasi-steady horizontal heat transfer predicted in the 3-D simulation is slightly higher than that predicted in the 2-D simulation. The difference in the time-averaged values (for $t$ = 0.18 to 0.22) is about 6%. It is also noteworthy that the calculated heat transfer from the 3-D simulation fluctuates at smaller amplitude than that from the 2-D simulation at both the transitional and quasi-steady stages. This is because the heat transfer from the 3-D simulation is averaged over the transverse direction, whereas that from the 2-D simulation is representative of the values on a single sectional plane.

## Conclusions

The temperature structures in a water-filled shallow wedge subject to solar radiation are revealed based on numerical solutions of both 2-D and 3-D governing equations. The results verify an early claim based on a 2-D calculation that the flow development from an isothermal and stationary state passes through three stages, an initial growth stage, a transitional stage and a quasi-steady stage [5]. In the initial and early transitional stages, the flow is essentially 2-D, and it becomes 3-D at later stages. It is interesting to see from the present comparison between the 2-D and 3-D simulations that the 2-D simulation reproduces the major flow features at all stages irrespective of the three-dimensionality, and it predicts a horizontal heat transfer rate which is sufficiently close to the 3-D prediction. Therefore, the 2-D model can be used to extract additional flow details with confidence. However, the nature of the 2-D model does not allow a full resolution of the detail of the secondary convection.


## Acknowledgement

This research was financially supported by the Australian Research Council (ARC).


## References


[1] Farrow, D.E. & Patterson, J.C., The daytime circulation and temperature structure in a reservoir sidearm, *International Journal of Heat and Mass Transfer*, **37**, 1994, 1957-1968.

[2] Foster T.D., Intermittent convection, *Geophysical Fluid Dynamics*, **2**, 1971, 201-217.

[3] Horsch, G.M., Stefan, H.G. & Gavali, S., Numerical simulation of cooling-induced convective currents on a littoral slope, *International Journal for Numerical Methods in Fluids*, **19**, 1994, 105-134.

[4] Lei, C., Cheng, L. & Kavanagh, K., Spanwise length effects on three-dimensional modelling of flow over a circular cylinder, *Computer Methods in Applied Mechanics and Engineering*, **190**, 2001, 2909-2923.

[5] Lei, C. & Patterson, J.C., A numerical simulation of the daytime natural convection in a reservoir sidearm, in *CHT'01: Advances in Computational Heat Transfer II*, editors G. de Vahl Davis & E. Leonardi, Begell House Inc, 2001, **2**, 745-752.

[6] Lei, C., Patterson, J.C. & Lee, M., Visualisation of natural convection in a reservoir sidearm subject to surface radiation, in *Proceedings of The 7th Australasia Heat and Mass Transfer Conference*, editors G.B. Brassington & J.C. Patterson, Chalkface Press P/L, 2000, 201-208.

[7] Monismith, S.G., Imberger, J. & Morison, M.L., Convective motions in the sidearm of a small reservoir, *Limnology & Oceanography*, **35**, 1990, 1676-1702.

[8] Rabl, A. & Nielsen, C.E., Solar ponds for space heating, *Solar Energy*, **17**, 1975, 1-12.